ACS APPLIED MATERIALS & INTERFACES

Research Article

www.acsami.org

Oxidation Resistance of Monolayer Group-IV Monochalcogenides

Yu Guo, Si Zhou,* Yizhen Bai, and Jijun Zhao

Key Laboratory of Materials Modification by Laser, Ion and Electron Beams, Dalian University of Technology, Ministry of Education, Dalian 116024, China

Supporting Information

ABSTRACT: Ridged, orthorhombic two-dimensional (2D) group-V elemental and group IV−VI compound analogues of phosphorene provide a versatile platform for nanoelectronics, optoelectronics, and clean energy. However, phosphorene is vulnerable to oxygen in ambient air, which is a major obstacle for its applications. Regarding this issue, here we explore the oxidation behavior of monolayer group-IV monochalcogenides (GeS, GeSe, SnS, and SnSe), in comparison to that of phosphorene and arsenene by first-principles calculations. We find superior oxidation resistance of the monolayer group-IV monochalcogenides, with activation energies for the chemisorption of O_2 on the 2D sheets in the range of 1.26−1.60 eV, about twice of the values of phosphorene and arsenene. The distinct oxidation behaviors of monolayer group-IV monochalcogenides and group-V phosphorene analogues originate from their different bond natures. Moreover, the chemisorption of a moderate amount of oxygen atoms does not severely deteriorate the electronic band structures of the monolayer group-IV monochalcogenides. These results shine light on the utilization of the monolayer group-IV monochalcogenides for next-generation 2D electronics and optoelectronics with high performance and stability.

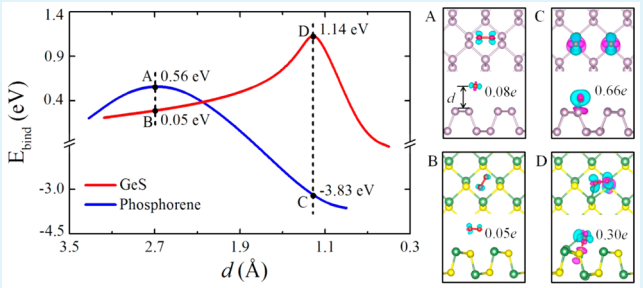

KEYWORDS: *monolayer group-IV monochalcogenides, oxidation resistance, activation energy, band gap, effective mass*

INTRODUCTION

The boom of graphene has stimulated an avalanche of 2D materials beyond graphene.[1−4] Phosphorene, the layered form of black phosphorus, possesses ideal band gap and high carrier mobility for electronics,[5−8] and leads to the exploration of an entirely new family of group-V elemental 2D materials, such as arsenene and antimonene with band gaps of 2.49 and 2.28 eV, respectively.[9−12] However, phosphorene suffers from its air instability, ascribed to the lone-pair electrons that favor oxygen bonding.[13] It was found that black phosphorus flakes are hydrophilic and easily oxidized in the air moisture,[14−16] which substantially degrades their physical properties and device performance.[17−23] Correspondingly, theoretical calculations reveal a relatively low activation energy of 0.54 eV[13] and a large exothermic reaction energy of 1.8−2.9 eV per oxygen atom for chemisorption of an O_2 molecule on the phosphorene surface[24,25] as well as fast migration of oxygen atom on phosphorene with a low diffusion barrier of 0.33 eV.[26]

Following the advancement of group-V elemental 2D materials, layered group-IV monochalcogenides, which are isoelectronic and isostructural to black phosphorus, are receiving increasing attentions due to their potential applications in high-sensitivity photodetectors,[27] field effect transistor,[28,29] photovoltaic cells,[30] memory switching devices,[31] thermoelectric devices,[32] anode materials for lithium ion battery,[33] flexible all-solid-state supercapacitors,[34] and electrochemical sensing.[35] They are also demonstrated as promising electrocatalysts for hydrogen evolution reactions as that for some other 2D chalcogenides materials.[35−38] To date, less toxic and earth-abundant GeS, GeSe, SnS, and SnSe nanosheets with thickness down to 1 nm have been synthesized in the laboratory.[27−31,33−35,39−45] One prominent merit of these kinds of 2D materials is their suitable band gaps, i.e., 1.6−1.7 eV for GeS,[28,35,39,45] 1.1−1.2 eV for GeSe,[39,45] 1.18−1.66 eV for SnS,[29,30] and 1.0−1.1 eV for SnSe,[31,41,43] which match the ideal energy for maximum absorption of incident solar radiation.

On the theoretical aspect, the structure, mechanical, and electronic properties of monolayer and few-layer group-IV monochalcogenides have been extensively investigated. The band gap of GeS, GeSe, SnS, and SnSe ranges from 1.44 to 2.32 eV for the monolayer sheets, and decreases with increasing thickness down to 1.00−1.24 eV for the bulk materials.[46,47] The monolayer group-IV monochalcogenides become direct band gap semiconductors when subjected to a small tensile strain (≤3%).[48] Their Young's moduli are anisotropic along armchair and zigzag directions with relatively low values of 7.8−57.63 GPa,[49] implying the potential for flexible devices. Their piezoelectric coefficients are surprisingly one to two orders of magnitude larger than the other frequently used piezoelectric materials.[50,51] They are demonstrated to be promising thermoelectric materials with low thermal conductivity of

Received: December 29, 2016
Accepted: March 13, 2017
Published: March 13, 2017

DOI: 10.1021/acsami.6b16786
ACS Appl. Mater. Interfaces 2017, 9, 12013−12020

only several $Wm^{-1}K^{-1}$ and a high figure of merit up to 3.27, and the thermoelectric performance can be improved by *p*- and *n*-type doping.[49,52]

In contrast to the comprehensive understanding of the oxidation of phosphorene, the oxidation processes of monolayer group-IV monochalcogenides are known very roughly. Reiss's group compared the oxidation behaviors of tin chalcogenide nanocrystals using Mössbauer spectroscopy. Their experiments reveal that SnTe nanocrystals are more vulnerable to oxidation than SnSe and SnS nanocrystals.[53] Yashina et al. and Deringer et al. reported that GeTe nanocrystals are readily oxidized in ambient air, and the Te-terminated surface is relatively more inert than the Ge-terminated counterparts.[54−59] The monolayer systems, however, have not been explored from either an experimental or theoretical aspect. The chemical stability of these novel 2D materials plays a vital role in their device performances.

Regarding the above critical issue, here we investigate for the first time the oxidation behaviors of monolayer group-IV monochalcogenides—GeS, GeSe, SnS, and SnSe, in comparison to that of group-V 2D elemental materials including phosphorene and arsenene. Our first-principles calculations show that the monolayer group-IV monochalcogenides are able to resist oxidation with large activation energies for the chemisorption of O_2 molecules. Even a low or intermediate content of oxygen atoms chemisorbed on the material surface does not severely degrade their electronic properties. These theoretical results not only help better understand the oxidation behaviors of monolayer group-IV monochalcogenides and group-V phosphorene analogues, and would stimulate the experimental fabrication of novel 2D devices of high performance.

COMPUTATIONAL METHODS

First-principles calculations were performed by spin polarized density functional theory[60] in the conjunction with projector augmented wave (PAW) potentials,[61,62] as implemented in the Vienna ab initio simulation package (VASP).[63] For exchange-correlation interactions, we used the generalized gradient approximation with the Perdew−Burke−Ernzerhof functional (GGA-PBE).[64] The energy cutoff for the plane-wave basis was chosen as 500 eV. The convergence criterion of total energy was set to 10^{-7} eV. The geometry optimization was considered to be converged when the residual force on each atom was less than 0.01 eV/Å. A vacuum region of 20 Å was added to the perpendicular direction to eliminate interaction between periodic images. Primitive unit cells were used to compute the fundamental electronic properties (such as band structures shown in Figure S1 of the Supporting Information, SI) of these 2D crystals, while a 5 × 4 supercell was used to describe the adsorption of an O_2 molecule. In both cases, uniform **k**-point meshes with spacings of 0.015/Å were adopted to sample the Brillouin zone. The climbing-image nudged elastic band (CI-NEB) method[65] was employed to investigate the adsorption and diffusion kinetics of O_2 molecule, and to determine the activation energy for chemisorption. Nine images were used to calculate the reaction path. The intermediate images of each CI-NEB simulation were relaxed until the perpendicular forces are smaller than 0.02 eV/Å.

RESULTS AND DISCUSSION

As shown in Figure 1, the monolayer group-IV monochalcogenides considered in this work—GeS, GeSe, SnS, and SnSe, share the same orthorhombic structure with group-V elemental monolayers (phosphorene and arsenene), that is, with hinge-like edges along the armchair direction. The lattice constants (*a*, *b* along *x* and *y* directions, respectively) and *b*/*a* ratio of

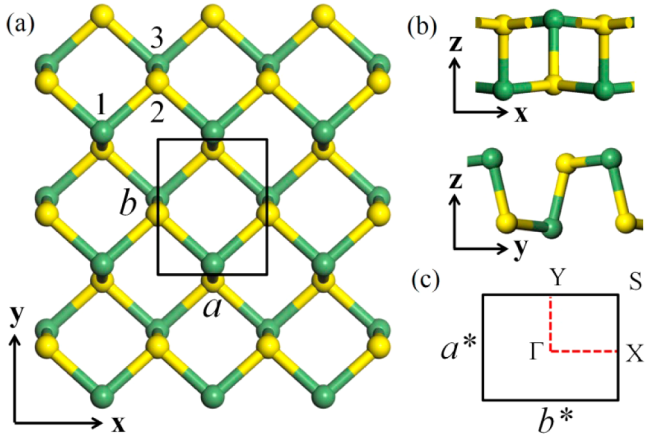

Figure 1. Lattice structure of monolayer group-IV monochalcogenides from (a) top and (b) side view. The unit cell with lattice parameters *a* and *b* is indicated by the black rectangular box in (a). The 2D Brillouin zone is shown in (c), with high-symmetry points labeled. The green and yellow balls represent the metal atoms and chalcogenide atoms, respectively.

these 2D materials are given by Table 1. Generally, the hinge-like orthorhombic structure yields larger lattice constant along armchair direction than that along zigzag direction, and the lattice anisotropy is characterized by *b*/*a* ratio. As presented in Table 1, the *b*/*a* ratio of the considered 2D orthorhombic structures follows *P* > As > GeS > GeSe > SnS > SnSe, implying less anisotropic structure and thus physical properties of monolayer group-IV monochalcogenides with regard to their group-V counterparts, as we will prove later.

The electronic band structures of these 2D monolayer materials are presented in Figure S1, and their band gaps and carrier effective masses are reported in Table 1. For group-IV monochalcogenides, GeS and SnS monolayers have larger band gaps than GeSe and SnSe, respectively. The top valence band (VB) and bottom conduction band (CB) of these groups IV−VI monolayers are highly dispersive (see Figure S1), giving carrier effective masses comparable to or even smaller than the values of phosphorene and arsenene. Generally speaking, all the considered phosphorene analogues show larger carrier effective masses along zigzag direction than armchair direction. For monolayer group-IV monochalcogenides, the effective masses are in the range of 0.14−2.03 m_0 for holes and 0.12−0.26 m_0 for electron, respectively. Such small effective masses indicate that the carriers are rather mobile in these 2D sheets. They show less anisotropy of carrier effective masses along *x* and *y* directions compared to phosphorene and arsenene; the anisotropy of the effective masses increases with *b*/*a* ratio; SnS and SnSe monolayers show nearly isotropic effective masses that are independent of the crystallographic orientation. In comparison, the group-V elemental monolayers have larger effective masses (phosphorene: 6.35 m_0 for hole and 1.27 m_0 for electron; arsenene: 1.56 m_0 for hole and 1.18 m_0 for electron) and stronger anisotropy. With the exception of the reduction of band gap with increasing number of layers, bilayer, and bulk group-IV monochalcogenides present electronic properties very similar to those of the monolayer systems, as demonstrated by Figure S2 and Table S1.

To characterize the chemical stability of monolayer group-IV monochalcogenides and group-V phosphorene analogues in the oxygen environment, we investigate the physisorption and chemisorption of an O_2 molecule on these 2D sheets and

DOI: 10.1021/acsami.6b16786
ACS Appl. Mater. Interfaces 2017, 9, 12013−12020

Table 1. Lattice Parameters (a, b) and Relative Ratio (b/a), Effective Masses of Hole (m^h) and Electron (m^e) along x and y Directions (m_0 is the Electron Rest Mass), and Band Gap (E_g) of Monolayer Group-IV Monochalcogenides, Phosphorene and Arsenene, Calculated Using the PBE Functional[a]

	a(Å)	b (Å)	b/a	m_x^h (m_0)	m_y^h (m_0)	m_x^e (m_0)	m_y^e (m_0)	E_g (eV) PBE	E_g (eV) HSE06
GeS	3.68	4.40	1.20	2.03 (3.95)	0.23 (0.35)	0.26 (0.47)	0.15 (0.66)	1.65 (1.67)	2.35
GeSe	3.99	4.26	1.07	0.33 (1.15)	0.16 (0.29)	0.23 (1.37))	0.14 (0.37)	1.14 (1.11)	2.03
SnS	4.09	4.26	1.04	0.28 (0.57)	0.21 (0.42)	0.20 (1.31)	0.19 (0.41)	1.45 (1.56)	2.15
SnSe	4.27	4.41	1.03	0.17 (1.44)	0.14 (0.12)	0.14 (1.40)	0.12 (0.17)	0.89 (0.97)	1.44
P	3.30	4.60	1.39	6.35 (24.28)	0.15 (0.17)	1.27 (1.63)	0.14 (0.18)	0.91 (0.97)	1.52
As	3.69	4.75	1.29	1.56 (2.50)	0.27 (0.34)	1.18 (1.42)	0.25 (0.11)	0.77 (0.79)	1.24

[a]The band gaps calculated by the HSE06 method are also listed for comparison. The data in brackets are effective masses for the oxidized monolayers as shown in the Figures 5 and S7, with oxygen concentration of about 0.6 oxygen atoms/nm^2.

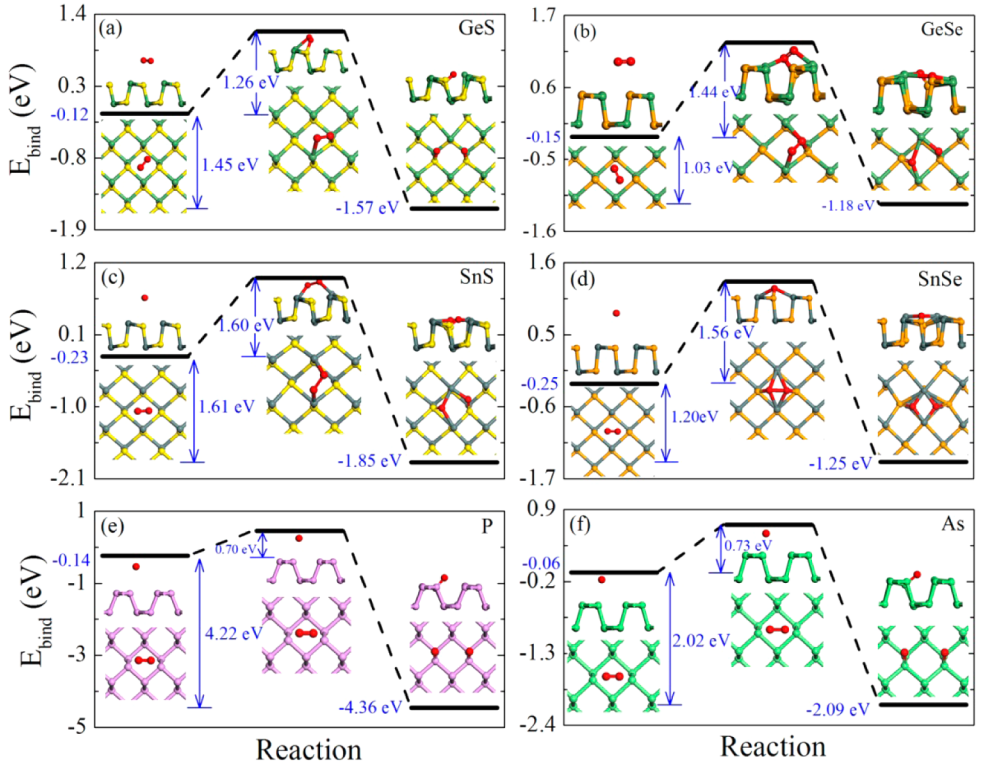

Figure 2. Reaction pathway for a physisorbed O_2 molecule to dissociate and chemisorb on the surface of (a) GeS, (b) GeSe, (c) SnS, (d) SnSe, (e) phosphorene, and (f) arsenene monolayer sheets, respectively. The black line segments indicate the energy levels of the initial state, transition state, and final state, respectively, with each corresponding atomic structures (top and side views) next to the energy level. The blue numbers give (from left to right) the binding energy of initial state, heat of reaction, activation energy, and binding energy of final state, respectively. The metal atoms and chalcogenide atoms are shown in green (dark green) and yellow (orange) colors, respectively, and the oxygen atom is shown in red.

simulate the dissociative oxidation processes. The interaction between O_2 and a monolayer is described by the binding energy (E_{bind}) defined as follows:

$$E_{bind} = E_{tot} - E_{monolayer} - E_{O2} \quad (1)$$

where E_{tot}, $E_{monolayer}$, and E_{O2} are the energies of monolayer phosphorene analogue adsorbed by an O_2 molecule, the pristine monolayer, and an individual O_2 molecule in the triplet state, respectively. By definition, a negative E_{bind} means the exothermic adsorption of O_2 molecule.

Figure 2 illustrates the dissociation processes for an O_2 molecule initially physisorbed on the phosphorene analogues into oxygen atoms chemisorbed on the monolayer sheets. The absorption configurations for the initial and final states are shown in Figure 2. In the situation of physisorption, O_2 molecule stays about 3 Å above the surface of phosphorene analogues with binding energy between −0.25 eV and −0.06 eV, and the binding energy does not sensitively depend on the specific location or orientation of the O_2 molecule. As the O_2 molecule approaches the 2D sheets, the O−O bond is elongated from 1.26 to 2.40 Å in the transition states (see Table S2). The O_2 molecule undergoes a transition from physisorption to chemisorption by overcoming an activation energy (E_a), which are 0.70 eV (0.73 eV) for phosphorene (arsenene) and 1.26−1.60 eV for monolayer group-IV monochalcogenides, respectively. The small activation energy for the chemisorption of O_2 on phosphorene (in agreement with a previous theoretical value of 0.54 eV[13]) indicates the easy oxidation of phosphorene in ambient air, which is consistent with the experimental observations.[14−20] Similar poor stability of arsenene in air is expected, as suggested by its small

DOI: 10.1021/acsami.6b16786
ACS Appl. Mater. Interfaces 2017, 9, 12013−12020

activation energy for O_2 chemisorption. In contrast, monolayer group-IV monochalcogenides show larger activation energies, about twice the values for phosphorene and arsenene, indicating much slower oxidation rates. The activation energy for monolayer group-IV monochalcogenides is comparable to that for perfect MoS_2 monolayer, which possesses high oxidation resistance with an activation energy of 1.59 eV for O_2 chemisorption.[66] We also considered monolayer GeTe and SnTe, and obtained activation energies of 1.10 and 0.92 eV, respectively (Figure S3). Their lower activation energies than the sulfide and selenide monolayers suggest that they are more vulnerable to oxidation, in qualitative agreement with the trend experimentally observed on the air stabilities of GeTe and SnTe nanocrystals.[53−59] Therefore, monolayer group-IV monochalcogenides including GeS, GeS, SnS, and SnSe show great potential as a new family of oxidation resistant 2D materials.

To characterize the thermodynamic stability of the oxidized products, we define heat of reaction as follows:

$$\Delta H = E_{\text{bind}}^{\text{phys}} - E_{\text{bind}}^{\text{chem}} \quad (2)$$

where $E_{\text{bind}}^{\text{phys}}$ and $E_{\text{bind}}^{\text{chem}}$ are the binding energies for O_2 physisorbed and chemisorbed on the 2D sheets in the equilibrium states, respectively. As displayed in Figure 2, we obtain ΔH of 1.20−1.61 eV for monolayer group-IV monochalcogenides, 4.22 and 2.02 eV for phosphorene and arsenene, respectively. Again, the smaller ΔH of monolayer group-IV monochalcogenides indicates weaker driving force for an O_2 molecule to dissociate and chemisorb on these 2D sheets, suggesting their higher resistivity to oxidation and superior chemical stability in ambient air. Even in a higher concentration of oxygen adsorption by using a smaller supercell, similar results of heat of reaction as well as activation energy are obtained by using GeS monolayer as an example (see S4 in the SI for details). We also considered bilayer group-IV monochalcogenides, and they show enhanced oxidation resistance compared to the monolayer systems (see SI S6), indicating the promising stabilities of group-IV monochalcogenides thin films. Our calculations are in good accord with the recent experimental observation that these novel 2D materials of group-IV monochalcogenides in air are stable over time without observable structural degeneration. Therefore, these monolayer group-IV monochalcogenides sustain the stability of device performance for long-term durability.[29,44]

Phosphorene is known to be chemically unstable in ambient air.[14−23] Experiments revealed that phosphorene rapidly degrades in the presence of both O_2 and H_2O, the degradation process slows down with exposure to O_2 only, and H_2O alone interact very weakly with pristine phosphorene.[20,21,67] The easy oxidation of phosphorene may be attributed to the well matched band gap and band-edge positions for the redox potential according to first-principles studies.[22,23,67,68] The oxidized phosphorene surface becomes superhydrophilic, which in turn aggravates the degradation process in air.[20,21,67] To examine the effect of humid environment, we perform a comparative simulation of the oxidation processes of monolayer GeS and phosphorene by putting a H_2O molecule nearby O_2. As shown in Figure 3, the H_2O molecule retains its physisorption on the 2D sheet during the entire reaction process and the positions of oxygen atoms are not influenced by H_2O, as compared with the situation without presence of H_2O (Figure 2). Here we redefine a binding energy (E_{bind}*) as follows:

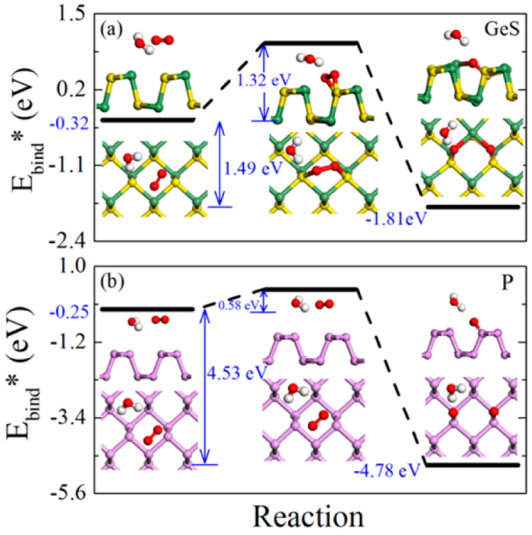

Figure 3. Reaction pathway for a physisorbed O_2 molecule to dissociate and chemisorb on the surface of (a) GeS and (b) phosphorene monolayer sheets nearby a H_2O molecule. The black line segments indicate the energy levels of the initial state, transition state, and final state, respectively, with each corresponding atomic structures (top and side views) next to the energy level. The blue numbers give (from left to right) the binding energy of initial state, heat of reaction, activation energy, and binding energy of final state, respectively. The H, O, P, S, and Ge atoms are shown in white, red, purple, yellow, and green colors, respectively.

$$E_{\text{bind}}{}^{*} = E_{\text{tot}} - E_{\text{monolayer}} - E_{\text{O2}} - E_{\text{H2O}} \quad (3)$$

where E_{H2O} is the energy of a H_2O molecule. Compared to the previous case without water, the binding energies for both initial and final states are reduced by about 0.11−0.42 eV, simply due to the hydrogen bond between the water molecule and one of the oxygen atom from O_2 molecule. With a H_2O molecule physisorbed nearby, the activation energy for O_2 chemisorption on phosphorene is 0.58 eV, about 0.12 eV lower than that with only presence of O_2 only, implying the acceleration oxidation of phosphorene in the humid environment. In contrast, the activation energy of 1.32 eV for oxygen dissociation on GeS monolayer in the presence of both O_2 and H_2O is only slightly higher than the circumstance without H_2O by 0.06 eV, which suggests that the water molecule does not influence the oxidization behavior of the GeS monolayer. The above results further validate the superior oxidation resistance of monolayer group-IV monochalcogenides.

The distinct chemical stabilities of monolayer group-IV monochalcogenides and group-V phosphorene analogues in the O_2 environment originate from their different bond natures, as revealed by Table 2. Phosphorene has covalent P−P bonds with bond overlap population[69] of 0.61 and 0.35 for the two P atoms on the same and different sublayers, respectively; a lone pair remains in one of the sp^3 orbitals, which are stereochemically active and vulnerable to oxidation reactions (see the projected density of states (PDOS) in Figure S7). In contrast, the GeS monolayer, as a representative of monolayer group-IV monochalcogenides, has polar Ge−S bonds with strong ionicity. The bond overlap population is 0.30 and 0.01 for the Ge/S atoms on the same and different sublayers, respectively. The frontier orbitals of the Ge and S atoms are strongly coupled with each other, as corroborated by the PDOS in Figure S5, accompanied by prominent charge transfer of 0.21

DOI: 10.1021/acsami.6b16786
ACS Appl. Mater. Interfaces 2017, 9, 12013−12020

Table 2. Bond Overlap Population for GeS, GeSe, SnS, SnSe, Phosphorene, and Arsenene Monolayer Sheets, Respectively[a]

material	bond population 1−2	bond population 2−3	charge transfer (e)
GeS	0.01	0.30	0.21
GeSe	0.18	0.38	0.13
SnS	0.35	0.36	0.21
SnSe	0.37	0.37	0.18
P	0.61	0.35	--
As	0.75	0.39	--

[a]"1-2" and "2-3" represent the bonds between two adjacent atoms in the same sublayer and in two different sublayers, respectively (see Fig. 1). The charge transfer from metal atoms to chalcogenide atoms is also given for the GeS, GeSe, SnS, and SnSe monolayers by Hirshfeld charge analysis.[70]

e from Ge to S atom. These highly polar Ge−S bonds, distinct from the P−P bonds with lone pairs in phosphorene, less favor the interaction with the adsorbed O_2 molecules, and thus exhibit superior resistance to oxidation.

More atomistic insights can be gained from the discrepant mechanisms of the oxidation processes for phosphorene and GeS monolayer, as illustrated by Figure 4. The oxidation reaction for phosphorene involves a transition state, where the O_2 molecule is physisorbed at a distance of 2.70 Å from the monolayer with E_{bind} = 0.54 eV (point A in Figure 4). Further approaching of the physisorbed O_2 molecule to the phosphorene surface continuously lowers the energy of the system owing to the lone pairs that favor the interaction with O_2. An auxiliary state (point C in Figure 4), where O_2 chemically bonds to the P atoms with bond length of 1.73 Å, shows large charge transfer of 0.66 e from the P to O atom and E_{bind} as low as −3.83 eV. However, the GeS monolayer undergoes a transition state where O_2 is chemisorbed on the monolayer (O−Ge bond length = 2.00 Å, point D in Figure 4). Less charge transfer of 0.30 e occurs from the Ge to O atom due to the strong ionicity of Ge−S bonds. As a consequence, the energy of system is raised to E_{bind} = 1.14 eV, namely a large energy energy for the O_2 molecule to dissociate and form two chemisorbed O atoms on the GeS monolayer. Figure 4 presents a general mechanism for the distinct oxidation resistances between monolayer group-IV monochalcogenides and group-V phosphorene analogues. Similar bond nature and oxidation behaviors can be found in arsenene as that in phosphorene, and in the other group-IV 2D compounds as that in the GeS monolayer (see Figure 2 and Figure S8).

The monolayer group-IV monochalcogenides possess excellent oxidation resistance; and more importantly, a low content of oxygen chemisorbed on the 2D sheets would not severely affect their electronic properties. As revealed by Figure 5, the monolayer group-IV monochalcogenides chemisorbed by oxygen atoms with concentration of about 0.6 oxygen atoms/nm^2 preserve the electronic band structures of the pristine systems. The band gaps are intact and no impurity state is induced, as the interaction between oxygen atoms and the 2D sheets buries the frontier orbitals of oxygen atoms into deep energy levels. The band dispersions of VB and CB are only minorly changed, with the carrier effective masses in the range of 0.57−3.95 m_0 (0.47−1.40 m_0) along x direction, and 0.12−0.42 m_0 (0.17−0.66 m_0) along y direction for holes (electrons), which approach or are even lower than the values of pristine systems, as illustrated by Table 1. Therefore, the carrier transport in monolayer group-IV monochalcogenides would not be severely disrupted upon the chemisorption of oxygen in low contents. Even with chemisorption of a high oxygen concentration (1.4 oxygen atoms/nm^2), the electronic properties of monolayer group-IV monochalcogenides in terms of band gap and carrier effective masses are not severely affected (the details are given in Figure S5 and Table S3). In comparison, the electronic properties of phosphorene and arsenene are more vulnerable by the chemisorption of oxygen (see Figure S9). For oxidized phosphorene, the band dispersion of CB along x direction is substantially flattened, with the hole effective mass increased to 24.28 m_0, almost four times of the value of pristine monolayer. Similarly, oxidized arsenene has hole effective mass of 2.50 m_0 along x direction, about twice of the pristine value. Also note that we have considered several other chemisorption sites for oxygen and obtained similar results on the electronic properties (see S10 in the SI for details).

CONCLUSIONS

We explore the oxidation behaviors of monolayer group-IV monochalcogenides by comprehensive first-principles calcula-

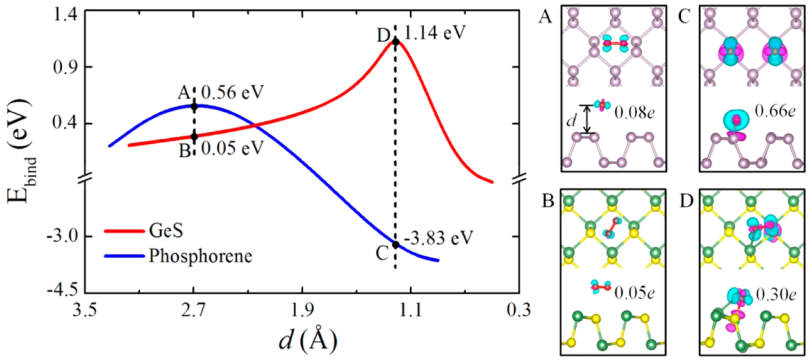

Figure 4. Mechanism of discrepant oxidation resistances of phosphorene and the GeS monolayer. The left panel schematically shows the binding energy (E_{bind}) of an O_2 molecule adsorbed on phosphorene and the GeS monolayer as a function of the distance (d) to the monolayer. Parts "A" and "D" indicate the transition states obtained by NEB search; and parts "B" and "C" are two auxiliary states for comparison. The corresponding structures, differential charge densities and charge transfer are shown on the right panels. P, Ge, and S atoms are represented in purple, green, and yellow colors, respectively. The cyan and magenta indicate the electron accumulation and depletion regions, respectively, with isosurface value of 0.006 lel per Å^3.

DOI: 10.1021/acsami.6b16786
ACS Appl. Mater. Interfaces 2017, 9, 12013−12020

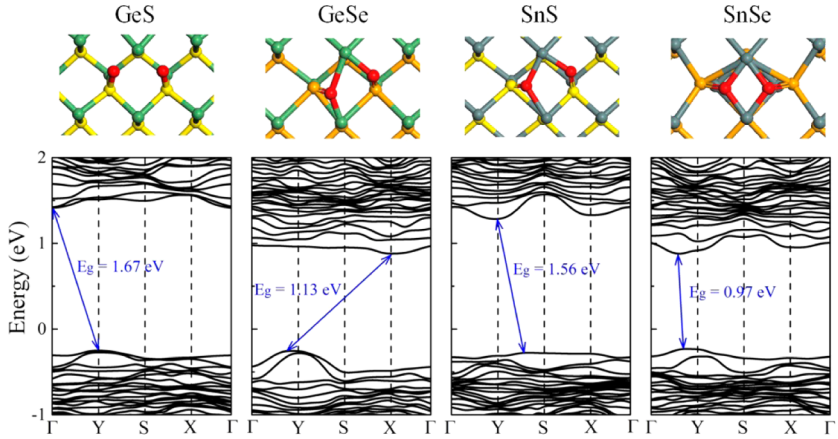

Figure 5. Local atomic geometries (top panels) and electronic band structures (bottom panels) of GeS, GeSe, SnSe, and SnS monolayers chemisorbed by two oxygen atoms per supercell. A 5 × 4 supercell is used for all the systems. E_g is the band gap denoted by the solid arrow. The representation of high-symmetry points of the first Brillouin zone are illustrated in Figure 1(c).

tions. Compared to phosphorene and arsenene, monolayer group-IV monochalcogenides can better withstand oxidation in the ambient air with or without humidity. The dissociation and chemisorption of O_2 on monolayer group-IV monochalcogenides are kinetically difficult in both dry and humid conditions involving activation energies of 1.26−1.60 eV, about twice of the values of phosphorene and arsenene. The different bond natures between monolayer group-IV monochalcogenides and group-V phosphorene analogue result in their distinct oxidation behaviors. These 2D compound sheets consist of polar covalent bonds between the group IV and VI atoms, which less favor interaction and charge transfer with the adsorbed O_2 molecules compared to the P−P bonds with lone pairs in phosphorene. Therefore, monolayer group-IV monochalcogenides show large energy barriers for dissociation and chemisorption of O_2 molecules and are resistant to oxidation. Noticeably, a low or intermediate content of oxygen atoms chemisorbed on the monolayer group-IV monochalcogenides does not severely affect the electronic properties of the systems: the band gaps are intact in absence of any impurity states, and the carrier effective masses are only moderately changed. Our theoretical results help better understand the chemical stability of monolayer group-IV monochalcogenides and group-V phosphorene analogues in ambient air, and open the opportunity to fabricate high-performance thermoelectric and photovoltaic devices by utilizing these oxidation-resistant and earth-abundant 2D materials.

■ ASSOCIATED CONTENT

Supporting Information

The Supporting Information is available free of charge on the ACS Publications website at DOI: 10.1021/acsami.6b16786.

Band structures of monolayer, bilayer and bulk phosphorene analogues, O—O bond length in transition and final states, dissociation of O_2 on monolayer GeTe and SnTe, bilayer group-IV monochalcogenides, and on monolayer group-IV monochalcogenides with moderate O_2 concentration, density of states of phosphorene and monolayer group-IV monochalcogenides, atomic structure and charge density difference of the transition state for dissociation of O_2, band structures of oxidized monolayers, and supplementary references (PDF)

■ AUTHOR INFORMATION

Corresponding Author

*E-mail: sizhou@dlut.edu.cn (S.Z.).

ORCID

Si Zhou: 0000-0002-0842-1075

Jijun Zhao: 0000-0002-3263-7159

Notes

The authors declare no competing financial interest.

■ ACKNOWLEDGMENTS

This work was supported by the National Natural Science Foundation of China (11504041, 11574040), the China Postdoctoral Science Foundation (2015M570243, 2016T90216), the Fundamental Research Funds for the Central Universities of China (DUT15RC(3)014, DUT16-LAB01), and the Supercomputing Center of Dalian University of Technology.

■ REFERENCES

(1) Pan, Y.; Zhang, L.; Huang, L.; Li, L.; Meng, L.; Gao, M.; Huan, Q.; Lin, X.; Wang, Y.; Du, S.; Freund, H.-J.; Gao, H.-J. Construction of 2D Atomic Crystals on Transition Metal Surfaces: Graphene, Silicene, and Hafnene. *Small* **2014**, *10*, 2215−2225.

(2) Balendhran, S.; Walia, S.; Nili, H.; Sriram, S.; Bhaskaran, M. Elemental Analogues of Graphene: Silicene, Germanene, Stanene, and Phosphorene. *Small* **2015**, *11*, 640−652.

(3) Xu, M.; Liang, T.; Shi, M.; Chen, H. Graphene-Like Two-Dimensional Materials. *Chem. Rev.* **2013**, *113*, 3766−3798.

(4) Tang, Q.; Zhou, Z. Graphene-Analogous Low-Dimensional Materials. *Prog. Mater. Sci.* **2013**, *58*, 1244−1315.

(5) Tran, V.; Soklaski, R.; Liang, Y.; Yang, L. Layer-Controlled Band Gap and Anisotropic Excitons in Few-Layer Black Phosphorus. *Phys. Rev. B: Condens. Matter Mater. Phys.* **2014**, *89*, 235319.

(6) Qiao, J.; Kong, X.; Hu, Z.-X.; Yang, F.; Ji, W. High-Mobility Transport Anisotropy and Linear Dichroism in Few-Layer Black Phosphorus. *Nat. Commun.* **2014**, *5*, 4475.

(7) Liu, H.; Neal, A. T.; Zhu, Z.; Luo, Z.; Xu, X.; Tománek, D.; Ye, P. D. Phosphorene: An Unexplored 2D Semiconductor with a High Hole Mobility. *ACS Nano* **2014**, *8*, 4033−4041.

(8) Guo, Y.; Zhou, S.; Zhang, J.; Bai, Y.; Zhao, J. Atomic Structures and Electronic Properties of Phosphorene Grain Boundaries. *2D Mater.* **2016**, *3*, 025008.

(9) Zhang, S.; Xie, M.; Li, F.; Yan, Z.; Li, Y.; Kan, E.; Liu, W.; Chen, Z.; Zeng, H. Semiconducting Group 15 Monolayers: A Broad Range of

DOI: 10.1021/acsami.6b16786
ACS Appl. Mater. Interfaces 2017, 9, 12013−12020

Band Gaps and High Carrier Mobilities. *Angew. Chem.* **2016**, *128*, 1698−1701.
(10) Zhang, S.; Yan, Z.; Li, Y.; Chen, Z.; Zeng, H. Atomically Thin Arsenene and Antimonene: Semimetal−Semiconductor and Indirect−Direct Band-Gap Transitions. *Angew. Chem., Int. Ed.* **2015**, *54*, 3112−3115.
(11) Huo, C.; Sun, X.; Yan, Z.; Song, X.; Zhang, S.; Xie, Z.; Liu, J.-Z.; Ji, J.; Jiang, L.; Zhou, S.; Zeng, H. Few-Layer Antimonene: Large Yield Synthesis, Exact Atomical Structure and Outstanding Optical Limiting. *J. Am. Chem. Soc.* **2017**, *139*, 3568.
(12) Ji, J.; Song, X.; Liu, J.; Yan, Z.; Huo, C.; Zhang, S.; Su, M.; Liao, L.; Wang, W.; Ni, Z.; Hao, Y.; Zeng, H. Two-Dimensional Antimonene Single Crystals Grown by van der Waals Epitaxy. *Nat. Commun.* **2016**, *7*, 13352.
(13) Ziletti, A.; Carvalho, A.; Campbell, D. K.; Coker, D. F.; Castro Neto, A. H. Oxygen Defects in Phosphorene. *Phys. Rev. Lett.* **2015**, *114*, 046801.
(14) Koenig, S. P.; Doganov, R. A.; Schmidt, H.; Castro Neto, A. H.; Özyilmaz, B. Electric Field Effect in Ultrathin Black Phosphorus. *Appl. Phys. Lett.* **2014**, *104*, 103106.
(15) Castellanos-Gomez, A.; Vicarelli, L.; Prada, E.; Island, J. O.; Narasimha-Acharya, K. L.; Blanter, S. I.; Groenendijk, D. J.; Buscema, M.; Steele, G. A.; Alvarez, J. V.; Zandbergen, H. W.; Palacios, J. J.; van der Zant, H. S. J. Isolation and Characterization of Few-Layer Black Phosphorus. *2D Mater.* **2014**, *1*, 025001.
(16) Woomer, A. H.; Farnsworth, T. W.; Hu, J.; Wells, R. A.; Donley, C. L.; Warren, S. C. Phosphorene: Synthesis, Scale-up, and Quantitative Optical Spectroscopy. *ACS Nano* **2015**, *9*, 8869−8884.
(17) Avsar, A.; Vera-Marun, I. J.; Tan, J. Y.; Watanabe, K.; Taniguchi, T.; Castro Neto, A. H.; Özyilmaz, B. Air-Stable Transport in Graphene-Contacted, Fully Encapsulated Ultrathin Black Phosphorus-Based Field-Effect Transistors. *ACS Nano* **2015**, *9*, 4138−4145.
(18) Buscema, M.; Groenendijk, D. J.; Blanter, S. I.; Steele, G. A.; van der Zant, H. S. J.; Castellanos-Gomez, A. Fast and Broadband Photoresponse of Few-Layer Black Phosphorus Field-Effect Transistors. *Nano Lett.* **2014**, *14*, 3347−3352.
(19) Ma, X.; Lu, W.; Chen, B.; Zhong, D.; Huang, L.; Dong, L.; Jin, C.; Zhang, Z. Performance Change of Few Layer Black Phosphorus Transistors in Ambient. *AIP Adv.* **2015**, *5*, 107112.
(20) Favron, A.; Gaufres, E.; Fossard, F.; Phaneuf-L'Heureux, A.-L.; Tang, N. Y. W.; Levesque, P. L.; Loiseau, A.; Leonelli, R.; Francoeur, S.; Martel, R. Photooxidation and Quantum Confinement Effects in Exfoliated Black Phosphorus. *Nat. Mater.* **2015**, *14*, 826−832.
(21) Yang, B.; Wan, B.; Zhou, Q.; Wang, Y.; Hu, W.; Lv, W.; Chen, Q.; Zeng, Z.; Wen, F.; Xiang, J.; Yuan, S.; Wang, J.; Zhang, B.; Wang, W.; Zhang, J.; Xu, B.; Zhao, Z.; Tian, Y.; Liu, Z. Te-Doped Black Phosphorus Field-Effect Transistors. *Adv. Mater.* **2016**, *28*, 9408−9415.
(22) Zhou, Q.; Chen, Q.; Tong, Y.; Wang, J. Light-Induced Ambient Degradation of Few-Layer Black Phosphorus: Mechanism and Protection. *Angew. Chem.* **2016**, *128*, 11609−11613.
(23) Zhao, Y.; Zhou, Q.; Li, Q.; Yao, X.; Wang, J. Passivation of Black Phosphorus via Self-Assembled Organic Monolayers by van der Waals Epitaxy. *Adv. Mater.* **2017**, *29*, 1603990.
(24) Wang, G.; Slough, W. J.; Pandey, R.; Karna, S. P. Degradation of Phosphorene in Air: Understanding at Atomic Level. *2D Mater.* **2016**, *3*, 025011.
(25) Ziletti, A.; Carvalho, A.; Trevisanutto, P. E.; Campbell, D. K.; Coker, D. F.; Castro Neto, A. H. Phosphorene Oxides: Bandgap Engineering of Phosphorene by Oxidation. *Phys. Rev. B: Condens. Matter Mater. Phys.* **2015**, *91*, 085407.
(26) Wang, G.; Pandey, R.; Karna, S. P. Phosphorene Oxide: Stability and Electronic Properties of a Novel Two-Dimensional Material. *Nanoscale* **2015**, *7*, 524−531.
(27) Mukherjee, B.; Cai, Y.; Tan, H. R.; Feng, Y. P.; Tok, E. S.; Sow, C. H. Nir Schottky Photodetectors Based on Individual Single-Crystalline GeSe Nanosheet. *ACS Appl. Mater. Interfaces* **2013**, *5*, 9594−9604.
(28) Ulaganathan, R. K.; Lu, Y.-Y.; Kuo, C.-J.; Tamalampudi, S. R.; Sankar, R.; Boopathi, K. M.; Anand, A.; Yadav, K.; Mathew, R. J.; Liu, C.-R.; Chou, F. C.; Chen, Y.-T. High Photosensitivity and Broad Spectral Response of Multi-Layered Germanium Sulfide Transistors. *Nanoscale* **2016**, *8*, 2284−2292.
(29) Deng, Z.; Cao, D.; He, J.; Lin, S.; Lindsay, S. M.; Liu, Y. Solution Synthesis of Ultrathin Single-Crystalline SnS Nanoribbons for Photodetectors via Phase Transition and Surface Processing. *ACS Nano* **2012**, *6*, 6197−6207.
(30) Liu, X.; Li, Y.; Zhou, B.; Wang, X.; Cartwright, A. N.; Swihart, M. T. Shape-Controlled Synthesis of SnE (E = S, Se) Semiconductor Nanocrystals for Optoelectronics. *Chem. Mater.* **2014**, *26*, 3515−3521.
(31) Vaughn, D. D.; In, S.-I.; Schaak, R. E. A Precursor-Limited Nanoparticle Coalescence Pathway for Tuning the Thickness of Laterally-Uniform Colloidal Nanosheets: the Case of SnSe. *ACS Nano* **2011**, *5*, 8852−8860.
(32) Zhao, L.-D.; Lo, S.-H.; Zhang, Y.; Sun, H.; Tan, G.; Uher, C.; Wolverton, C.; Dravid, V. P.; Kanatzidis, M. G. Ultralow Thermal Conductivity and High Thermoelectric Figure of Merit in SnSe Crystals. *Nature* **2014**, *508*, 373−377.
(33) Lu, J.; Nan, C.; Li, L.; Peng, Q.; Li, Y. Flexible SnS Nanobelts: Facile Synthesis, Formation Mechanism and Application in Li-Ion Batteries. *Nano Res.* **2013**, *6*, 55−64.
(34) Zhang, C.; Yin, H.; Han, M.; Dai, Z.; Pang, H.; Zheng, Y.; Lan, Y.-Q.; Bao, J.; Zhu, J. Two-Dimensional Tin Selenide Nanostructures for Flexible All-Solid-State Supercapacitors. *ACS Nano* **2014**, *8*, 3761−3770.
(35) Tan, S. M.; Chua, C. K.; Sedmidubsky, D.; Sofer, Z. k.; Pumera, M. Electrochemistry of Layered GaSe and GeS: Applications to ORR, OER and HER. *Phys. Chem. Chem. Phys.* **2016**, *18*, 1699−1711.
(36) Mohamad Latiff, N.; Wang, L.; Mayorga-Martinez, C. C.; Sofer, Z.; Fisher, A. C.; Pumera, M. Valence and Oxide Impurities in MoS_2 and WS_2 Dramatically Change Their Electrocatalytic Activity Towards Proton Reduction. *Nanoscale* **2016**, *8*, 16752−16760.
(37) Wang, Y.; Sofer, Z.; Luxa, J.; Pumera, M. Lithium Exfoliated Vanadium Dichalcogenides (VS_2, VSe_2, VTe_2) Exhibit Dramatically Different Properties from Their Bulk Counterparts. *Adv. Mater. Interfaces* **2016**, *3*, 1600433.
(38) He, Z.; Que, W. Molybdenum Disulfide Nanomaterials: Structures, Properties, Synthesis and Recent Progress on Hydrogen Evolution Reaction. *Appl. Mater. Today* **2016**, *3*, 23−56.
(39) Vaughn, D. D., II; Patel, R. J.; Hickner, M. A.; Schaak, R. E. Single-Crystal Colloidal Nanosheets of GeS and GeSe. *J. Am. Chem. Soc.* **2010**, *132*, 15170−15172.
(40) Zhao, S.; Wang, H.; Zhou, Y.; Liao, L.; Jiang, Y.; Yang, X.; Chen, G.; Lin, M.; Wang, Y.; Peng, H.; Liu, Z. Controlled Synthesis of Single-Crystal SnSe Nanoplates. *Nano Res.* **2015**, *8*, 288−295.
(41) Li, L.; Chen, Z.; Hu, Y.; Wang, X.; Zhang, T.; Chen, W.; Wang, Q. Single-Layer Single-Crystalline SnSe Nanosheets. *J. Am. Chem. Soc.* **2013**, *135*, 1213−1216.
(42) Liu, J.; Huang, Q.; Qian, Y.; Huang, Z.; Lai, F.; Lin, L.; Guo, M.; Zheng, W.; Qu, Y. Screw Dislocation-Driven Growth of the Layered Spiral-Type SnSe Nanoplates. *Cryst. Growth Des.* **2016**, *16*, 2052−2056.
(43) Ma, X.-H.; Cho, K.-H.; Sung, Y.-M. Growth Mechanism of Vertically Aligned SnSe Nanosheets via Physical Vapour Deposition. *CrystEngComm* **2014**, *16*, 5080−5086.
(44) Li, C.; Huang, L.; Snigdha, G. P.; Yu, Y.; Cao, L. Role of Boundary Layer Diffusion in Vapor Deposition Growth of Chalcogenide Nanosheets: The CaSe of GeS. *ACS Nano* **2012**, *6*, 8868−8877.
(45) Ramasamy, P.; Kwak, D.; Lim, D.-H.; Ra, H.-S.; Lee, J.-S. Solution Synthesis of GeS and GeSe Nanosheets for High-Sensitivity Photodetectors. *J. Mater. Chem. C* **2016**, *4*, 479−485.
(46) Huang, L.; Wu, F.; Li, J. Structural Anisotropy Results in Strain-Tunable Electronic and Optical Properties in Monolayer GeX and SnX (X = S, Se, Te). *J. Chem. Phys.* **2016**, *144*, 114708.
(47) Gomes, L. C.; Carvalho, A. Phosphorene Analogues: Isoelectronic Two-Dimensional Group-IV Monochalcogenides with

DOI: 10.1021/acsami.6b16786
ACS Appl. Mater. Interfaces 2017, 9, 12013−12020

Orthorhombic Structure. *Phys. Rev. B: Condens. Matter Mater. Phys.* **2015**, *92*, 085406.
(48) Kamal, C.; Chakrabarti, A.; Ezawa, M. Direct Band Gaps in Group IV-VI Monolayer Materials: Binary Counterparts of Phosphorene. *Phys. Rev. B: Condens. Matter Mater. Phys.* **2016**, *93*, 125428.
(49) Qin, G.; Qin, Z.; Fang, W.-Z.; Zhang, L.-C.; Yue, S.-Y.; Yan, Q.-B.; Hu, M.; Su, G. Diverse Anisotropy of Phonon Transport in Two-Dimensional Group IV-VI Compounds: A Comparative Study. *Nanoscale* **2016**, *8*, 11306−11319.
(50) Gomes, L. C.; Carvalho, A.; Castro Neto, A. H. Enhanced Piezoelectricity and Modified Dielectric Screening of Two-Dimensional Group-IV Monochalcogenides. *Phys. Rev. B: Condens. Matter Mater. Phys.* **2015**, *92*, 214103.
(51) Fei, R.; Li, W.; Li, J.; Yang, L. Giant Piezoelectricity of Monolayer Group IV Monochalcogenides: SnSe, SnS, GeSe, and GeS. *Appl. Phys. Lett.* **2015**, *107*, 173104.
(52) Wang, F. Q.; Zhang, S.; Yu, J.; Wang, Q. Thermoelectric Properties of Single-Layered SnSe Sheet. *Nanoscale* **2015**, *7*, 15962−15970.
(53) de Kergommeaux, A.; Faure-Vincent, J.; Pron, A.; de Bettignies, R.; Malaman, B.; Reiss, P. Surface Oxidation of Tin Chalcogenide Nanocrystals Revealed by 119Sn−Mössbauer Spectroscopy. *J. Am. Chem. Soc.* **2012**, *134*, 11659−11666.
(54) Deringer, V. L.; Lumeij, M.; Dronskowski, R. Ab Initio Modeling of α-GeTe(111) Surfaces. *J. Phys. Chem. C* **2012**, *116*, 15801−15811.
(55) Yashina, L. V.; Kobeleva, S. P.; Shatalova, T. B.; Zlomanov, V. P.; Shtanov, V. I. XPS Study of Fresh and Oxidized GeTe and (Ge,Sn)Te Surface. *Solid State Ionics* **2001**, *141−142*, 513−522.
(56) Yashina, L. V.; Püttner, R.; Neudachina, V. S.; Zyubina, T. S.; Shtanov, V. I.; Poygin, M. V. Poygin X-Ray Photoelectron Studies of Clean and Oxidized α-GeTe(111) Surfaces. *J. Appl. Phys.* **2008**, *103*, 094909.
(57) Deringer, V. L.; Dronskowski, R. Ab Initio Study of Molecular and Atomic Oxygen on GeTe(111) Surfaces. *J. Appl. Phys.* **2014**, *116*, 173703.
(58) Yashina, L. V.; Kobeleva, S. P.; Neudachina, V. S.; Shatalova, T. B.; Zlomanov, V. P. Xps Study of Fresh and Oxidized (Pb,Ge)Te Surfaces. *Surf. Interface Anal.* **2002**, *34*, 498−501.
(59) Deringer, V. L.; Dronskowski, R. From Atomistic Surface Chemistry to Nanocrystals of Functional Chalcogenides. *Angew. Chem., Int. Ed.* **2015**, *54*, 15334−15340.
(60) Kohn, W.; Sham, L. J. Self-Consistent Equations including Exchange and Correlation Effects. *Phys. Rev.* **1965**, *140*, A1133−A1138.
(61) Blöchl, P. E. Projector Augmented-Wave Method. *Phys. Rev. B: Condens. Matter Mater. Phys.* **1994**, *50*, 17953−17979.
(62) Kresse, G.; Joubert, D. From Ultrasoft Pseudopotentials to the Projector Augmented-Wave Method. *Phys. Rev. B: Condens. Matter Mater. Phys.* **1999**, *59*, 1758−1775.
(63) Kresse, G.; Furthmüller, J. Efficient Iterative Schemes for *Ab Initio* Total-Energy Calculations Using a Plane-Wave Basis Set. *Phys. Rev. B: Condens. Matter Mater. Phys.* **1996**, *54*, 11169−11186.
(64) Perdew, J. P.; Burke, K.; Ernzerhof, M. Generalized Gradient Approximation Made Simple. *Phys. Rev. Lett.* **1996**, *77*, 3865−3868.
(65) Mills, G.; Jónsson, H.; Schenter, G. K. Reversible Work Transition State Theory: Application to Dissociative Adsorption of Hydrogen. *Surf. Sci.* **1995**, *324*, 305−337.
(66) KC, S.; Longo, R. C.; Wallace, R. M.; Cho, K. Surface Oxidation Energetics and Kinetics on Mos2Monolayer. *J. Appl. Phys.* **2015**, *117*, 135301.
(67) Huang, Y.; Qiao, J.; He, K.; Bliznakov, S.; Sutter, E.; Chen, X.; Luo, D.; Meng, F.; Su, D.; Decker, J.; Ji, W.; Ruoff, R. S.; Sutter, P. Interaction of Black Phosphorus with Oxygen and Water. *Chem. Mater.* **2016**, *28*, 8330−8339.
(68) Li, Q.; Zhou, Q.; Niu, X.; Zhao, Y.; Chen, Q.; Wang, J. Covalent Functionalization of Black Phosphorus from First-Principles. *J. Phys. Chem. Lett.* **2016**, *7*, 4540−4546.
(69) Segall, M. D.; Shah, R.; Pickard, C. J.; Payne, M. C. Population Analysis of Plane-Wave Electronic Structure Calculations of Bulk Materials. *Phys. Rev. B: Condens. Matter Mater. Phys.* **1996**, *54*, 16317−16320.
(70) Hirshfeld, F. L. Bonded-Atom Fragments for Describing Molecular Charge Densities. *Theor. Chim. Acta* **1977**, *44*, 129−138.

DOI: 10.1021/acsami.6b16786
ACS Appl. Mater. Interfaces 2017, 9, 12013−12020